HHS Public Access

Author manuscript

J Biomed Mater Res A. Author manuscript; available in PMC 2022 February 01.

Published in final edited form as:

J Biomed Mater Res A. 2022 February ; 110(2): 245–256. doi:10.1002/jbm.a.37280.

Tissue response, macrophage phenotype and intrinsic calcification induced by cardiovascular biomaterials: Can clinical regenerative potential be predicted in a rat subcutaneous implant model?

Madeline Cramer[a,b], **Jordan Chang**[b], **Hongshuai Li, MD, PhD**[c], **Aurelie Serrero, PhD**[d], **Mohammed El-Kurdi, PhD**[d], **Martijn Cox, PhD**[d], **Frederick J. Schoen, MD, PhD**[e,#], **Stephen F. Badylak, DVM, MD, PhD**[*,a,b,f,#]

[a]Department of Bioengineering, University of Pittsburgh, 3700 O'Hara Street, Pittsburgh, PA, 15261, USA

[b]McGowan Institute for Regenerative Medicine, University of Pittsburgh, 450 Technology Drive, Suite 300, Pittsburgh, PA 15219, USA

[c]Musculoskeletal Growth and Regeneration Laboratory, Department of Orthopedic Surgery, University of Pittsburgh, 450 Technology Drive, Suite 206, Pittsburgh, PA 15219, USA

[d]Xeltis BV, De Lismortel 31, 5612 AR Eindhoven, The Netherlands

[e]Department of Pathology, Brigham and Women's Hospital and Harvard Medical School, 75 Francis Street, Boston, MA 02115, USA

[f]Department of Surgery, School of Medicine, University of Pittsburgh, University of Pittsburgh Medical Center Presbyterian Hospital, 200 Lothrop Street, Pittsburgh, PA 15213, USA

Abstract

The host immune response to an implanted biomaterial, particularly the phenotype of infiltrating macrophages, is a key determinant of biocompatibility and downstream remodeling outcome. The present study used a subcutaneous rat model to compare the tissue response, including macrophage phenotype, remodeling potential and calcification propensity of a biologic scaffold composed of glutaraldehyde-fixed bovine pericardium (GF-BP), the standard of care for heart valve replacement, with those of an electrospun polycarbonate-based supramolecular polymer scaffold (ePC-UPy), urinary bladder extracellular matrix (UBM-ECM), and a polypropylene mesh (PP). The ePC-UPy and UBM-ECM materials induced infiltration of mononuclear cells throughout the thickness of the scaffold within 2 days and neovascularization at 14 days. GF-BP and PP elicited a balance of pro-inflammatory (M1-like) and anti-inflammatory (M2-like) macrophages, while UBM-ECM and ePC-UPy supported a dominant M2-like macrophage phenotype at all timepoints. Relative to GF-BP, ePC-UPy was markedly less susceptible to calcification for the 180 day duration of the study. UBM-ECM induced an archetypical

[*]**Corresponding author:** Stephen F. Badylak. 450 Technology Drive, Suite 300, Pittsburgh, PA 15219. Phone: (+1) 412-624-5252. badylaks@upmc.edu.
[#]Co-Senior authors

constructive remodeling response dominated by M2-like macrophages and the PP caused a typical foreign body reaction dominated by M1-like macrophages. The results of this study highlight the divergent macrophage and host remodeling response to biomaterials with distinct physical and chemical properties and suggest that the rat subcutaneous implantation model can be used to predict *in vivo* biocompatibility and regenerative potential for clinical application of cardiovascular biomaterials.

Keywords

bovine pericardium; endogenous tissue restoration; host response; macrophage phenotype; supramolecular polymer

INTRODUCTION

The success or failure of a biomaterial in the clinical setting is ultimately dependent upon the host tissue response following *in vivo* placement[1], a characteristic called *biocompatibility*. A definition for biocompatibility, widely accepted in the biomaterials and medical device communities[2,3], includes the phrase "*the ability of a material to perform with an appropriate host response in a specific application*", a concept that has been expanded to include biologically active biomaterials[4,5].

The host immune response elicited by implantation of a biomaterial is influenced by the physical and chemical properties of the material[1]. While cells of both the innate and adaptive immune system can contribute to the host response, the phenotype of responding macrophages is arguably the most important determinant of the downstream remodeling outcome[6,7]. Specifically, persistent pro-inflammatory (M1-like) macrophages are associated with a less favorable outcome characterized by dense fibrosis, scar tissue, and chronic inflammation[8,9]. In contrast, a rapid transition of infiltrating macrophages from an initial M1-like response to an M2-like phenotype is associated with a constructive remodeling response, characterized by a resolution of inflammation and deposition of more organized, site-appropriate tissue[10,11].

The present study used a subcutaneous rat model to investigate the *in vivo* tissue host response, including inflammation, neovascularization, macrophage phenotype, remodeling and calcification of a biologic scaffold composed of glutaraldehyde-fixed bovine pericardium (GF-BP), which is the standard of care for valve substitutes for heart valve replacement[12], to that of a synthetic scaffold (ePC-UPy) intended for use in endogenous tissue restoration (ETR). These materials were also compared to both a scaffold derived from porcine urinary bladder extracellular matrix (UBM-ECM) and a polypropylene (PP) mesh, which represent an archetypical example of a constructive remodeling response and a classical foreign body reaction, respectively[13]. Since calcification is a major contributing pathology in the clinical failure of bioprosthetic heart valves[14], the vulnerability to calcification of ePC-UPy, a material currently in early pediatric pulmonary heart valve clinical trials, was compared with that of GF-BP to further determine the suitability of the ETR-based material for cardiovascular applications.

MATERIALS AND METHODS

Materials

GF-BP was obtained from commercial-grade bioprosthetic valves processed with a proprietary anti-calcification treatment, typical of those used in contemporary cardiovascular surgery. The GF-BP was rinsed three times in 500ml of sterile saline for one minute each to remove residual free glutaraldehyde prior to use.

ePC-UPy is a polycarbonate-based bioabsorbable supramolecular polymer characterized by the 2-ureido-4[1H]-pyrimidinone (UPy) binding motif which was processed into micro-porous three-dimensional structural implants by electrospinning. ePC-UPy is part of the RestoreX™ material platform developed by Xeltis (Eindhoven, The Netherlands) to enable ETR in a variety of cardiovascular applications[15–17].

UBM-ECM was prepared as previously described[18], lyophilized and sterilized with ethylene oxide. Surgical mesh constructed of knitted PP monofilaments was used as supplied (Bard® Mesh, Becton, Dickinson and Company).

All materials were cut into 8mm discs with a biopsy punch in an aseptic environment to maintain sterility. Prior to implantation, each ePC-UPy disc was further submerged in normal saline and centrifuged at 4000 RPM for 5 min. The disc was then soaked in heparinized blood collected from adult mother rats at room temperature for 1 hr while shaking at 1Hz.

Dorsal subcutaneous implantation in rats

Animal studies were conducted in compliance with all regulations as set forth by the University of Pittsburgh's Institutional Animal Care and Use Committee. Female Sprague Dawley rats with 1-3 day old pups were obtained from Envigo (Indianapolis, IN).

When rat pups reached 3 weeks of age, they received dorsal subcutaneous implants of ePC-UPy, GF-BP, UBM-ECM or PP (n=4 animals per timepoint/group). Following a dorsal midline incision, the material discs were sutured with 7-0 Prolene to the adjacent panniculus carnosus muscle. Each animal received a total of four material implants with two placed bilaterally on each dorsal side. Animals were sacrificed at 2, 14, 21, 90 and 180 days. Implants with surrounding tissue were carefully dissected out and processed to evaluate the *in vivo* tissue responses. To simulate the effect of mechanical stress on calcification, additional ePC-UPy and GF-BP discs folded in half and sutured closed with 7-0 Prolene were also implanted and examined following removal at 21 days.

Histologic evaluation

Samples with surrounding tissue were formalin-fixed, embedded in paraffin and 5μm serial sections were cut. Sections were stained with either hematoxylin and eosin (H&E), Alizarin Red S or von Kossa stains according to standard procedures to visualize general morphology, cellular infiltration and calcification. Quantification of nuclei, which correlates with the number of cells, within each material was performed using an image analysis algorithm in QuPath. The quantification of cellularity within each material is normalized

to the cross sectional area of the implanted material. The area of quantification for the PP group comprised of the tissue between the fibers of the mesh since there is no cellular penetration within the PP material itself.

Immunolabeling (Immunohistochemistry)

Following deparaffinization, antigen retrieval was performed with citrate buffer (pH = 6) at 95-100°C for 20 min. Endogenous peroxidase activity was quenched with 3% H_2O_2 for 10 min prior to blocking at room temperature for 1 hr. Tissue sections were incubated overnight at 4°C with CD31 antibody demarcating endothelial cells (1:500, Abcam) or tissue non-specific alkaline phosphatase (ALP) antibody (1:250, Abcam). Slides were incubated with horseradish peroxidase-conjugated (HRP) secondary antibody (1:200, Sigma Aldrich), developed with ImmPACT™ DAB substrate (Vector Laboratories), and counterstained with hematoxylin. Quantification of CD31 immunolabeling was performed using an image analysis algorithm in QuPath.

Macrophage response was evaluated using primary antibodies for pan-macrophage marker (mouse anti-CD68, 1:150, Bio-Rad Laboratories) and indicators of M1-like (rabbit anti-TNFα, 1:100, Abcam) and M2-like (goat anti-CD206, 1:100, R&D Systems) macrophage phenotypes and HRP-conjugated secondary antibodies (1:100, Sigma Aldrich) in blocking buffer. Signal was generated with Opal Polymer HRP (Akoya Biosciences), and nuclei were visualized with DRAQ5 (Fisher Scientific) staining. Slides were imaged on the Zeiss Observer Z1 microscope. Three fields of view per slide were selected in areas of cellular infiltration into the implanted material to depict the phenotype of the resultant host response. Quantification of macrophage immunolabeling was accomplished with an image analysis algorithm in CellProfiler which verifies co-localization of positive immunolabeling with cell nuclei and therefore discounts signal due to autofluorescence.

Radiographic and micro-computed tomography analysis

Specimen radiography using Faxitron®, was conducted by American Preclinical Services (Minneapolis, MN) on ePC-UPy and GF-BP samples. Samples for the 90 and 180 day time point were cut in half transversally prior to radiographic scans. Micro-computed tomography (μCT) scans were performed with a vivaCT 40 scanner (Scanco Medical) on a subset of folded samples from the 21 day timepoint with the settings: energy 70 kV, intensity 114 μA, integration time 300 ms, and isotropic voxel size of 10.5 μm as described previously[19].

Statistical analysis

Quantitative outcomes were compared with a two-way analysis of variance (ANOVA) and post hoc Sidak test to determine differences between groups. All statistical analysis was performed using GraphPad Prism and p values <0.05 were considered statistically significant. Data are reported as mean ± standard error.

RESULTS

The temporal evolution of density and spatial distribution of cellular infiltration and neovascularization are distinctly different among the biomaterials studied

With the GF-BP, mononuclear cells were noted as early as 2 days post implantation within the material but were limited to the edges of implant adjacent to the recipient tissue (Figure 1). At 14 and 21 days there was a more robust cellular response to the GF-BP material than the ePC-UPy and PP materials, which continued to be distributed mainly in those areas close to the edges with only a small number of cells deep into the material (Figure 1, Supplemental Figure 1). Inflammation was markedly reduced at 180 days (Figure 1).

In contrast, an infiltrate of mononuclear cells diffusely penetrated the full thickness of the ePC-UPy material as early as 2 days after implantation (Figure 1). By 14-21 days this material had an approximate doubling of the cell density that consisted primarily of mononuclear leukocytes and a small number of multinucleate giant cells intercalating between the individual fibers of the polymer (Figure 1, Supplemental Figure 1). The cell density and distribution remained relatively constant throughout the study period, manifesting in higher cellularity within the ePC-UPy material at long time points when the cellularity of other implanted materials had diminished (Figure 1B).

The UBM-ECM sheet showed robust early infiltration of mononuclear cells into the site of implantation with significantly more cells compared to all other materials starting at 2 days post implantation and continuing through days 14-21 (Figure 1, Supplemental Figure 1). The intense cellular response thereafter subsided and by 90-180 days this material was degraded and replaced by *de novo* fibrous tissue (Figure 1). Fibers of the PP mesh became rapidly surrounded by a thick cell layer of mononuclear and multinucleate giant cells (Figure 1A) that consolidated into a typical foreign body fibrous capsule by 180 days (Figure 1A, Supplemental Figure 1). The cellularity of the plane of tissue between the mesh fibers remained relatively low and constant across all time points (Figure 1B).

Beginning at 14 days post implantation, the elicited neovascularization was markedly different among the biomaterials (Figure 2B). With GF-BP, $CD31^+$ endothelial cells were present and scattered at the interface of the GF-BP implant with host tissue beginning as early as 14 days (Figure 2B, Supplemental Figure 2), but microvessels with intraluminal red blood cells (RBC) had largely diminished at 90 and 180 days post-implantation and were found only on the edges of the material (Figure 2A & 2B). In contrast, at 14 days post-implantation, $CD31^+$ endothelial cells were identified deep within the ePC-UPy material consistent with early neovascularization (Figure 2B, Supplemental Figure 2). At 90 and 180 days, there was significantly more CD31+ blood vessels within ePC-UPy compared to other implanted materials (Figure 2B). The abundant and widely distributed microvasculature contained intraluminal RBC, suggesting continuity of these small blood vessels with the surrounding host tissue (Figure 2A, Supplemental Figure 2).

Robust neovascularization of the UBM-ECM scaffold was observed at 14 and 21 days after implantation as indicated by significantly more CD31+ blood vessels compared to all other groups (Figure 2B, Supplemental Figure 2). As host fibrous tissue was formed over time

and the implant was degraded, the neovasculature had diminished (Figure 2A & 2B). Sparse $CD31^+$ cells were found in the tissue between the PP mesh fibers beginning at 14 days, but histologically apparent neovascularization was absent (Figure 2A & 2B, Supplemental Figure 2).

Macrophage phenotype differs markedly among the biomaterials studied

Macrophage phenotype was evaluated by immunolabeling for $CD68^+$, $TNF\alpha^+$ and $CD206^+$ cells (Figure 3A). The total numbers of $CD68^+CD206^+$, $CD68^+CD206^+TNF\alpha^+$, and $CD68^+TNF\alpha^+$ macrophages and the ratio of M2-like ($CD68^+CD206^+$) and M1-like ($CD68^+TNF\alpha^+$) macrophages was used to determine the dominant phenotype within the material (Figure 3B) and character of the inflammatory response (Figure 3C).

The macrophage phenotype present at the surfaces of the GF-BP material was approximately equal between M2-like and M1-like at all time points throughout the study (Figure 3B). The 21 day time point showed the greatest number of macrophages at the periphery of the GF-BP scaffold; the macrophages were markedly diminished by 180 days (Figure 3A & 3C).

In contrast, at all timepoints the ePC-UPy material was associated with a dominant M2-like macrophage phenotype (Figure 3B) that primarily reflected a paucity of $CD68^+TNF\alpha^+$ pro-inflammatory macrophages rather than an abundance of $CD68^+CD206^+$ cells (Figure 3C). The macrophages were distributed throughout the full thickness of the ePC-UPy material and were relatively constant in density from 14 to 180 days after implantation (Figure 3A & 3C).

The UBM-ECM scaffold promoted a predominately M2-like macrophage phenotype at all time points (Figure 3B). The UBM-ECM implant promoted a robust macrophage response at 2 and 14 days that began to decrease after 21 days (Figure 3C). The PP mesh induced a predominant M1-like macrophage ratio (Figure 3B). The macrophage response to the PP fibers was maximal at 14 days post-implantation and then decreased at longer time points (Figure 3C).

Susceptibility to calcification differs between materials

Radiography and μCT of GF-BP specimens revealed focal calcific deposits in nearly all of the twenty non-folded specimens with those in the longest duration specimens becoming grossly nodular; in contrast, only five of the twenty non-folded ePC-UPy polymer specimens had a suggestion of small focal calcific deposits by radiography (representative results in Figure 4A) but not by μCT. Histologically, three of the twenty GF-BP specimens showed calcification deep to the surface, which is consistent with the typical pattern observed in pericardial bioprosthetic valve material (Figure 4B)[20,21]. No calcification was observed in ePC-UPy specimens by histologic analysis (Figure 4C). Alizarin Red and ALP staining did not yield contributory information (Supplemental Figures 3 and 4). Neither UBM-ECM nor PP showed any calcification on routine light histologic sections (Figure 4A).

Folding of the GF-BP material to generate static strain within the material (simulating stress concentrations that occur during *in vivo* function) promoted extensive calcification

encompassing a major fraction of the 21 day implant, demonstrated by radiographic analysis (Figure 5A), μCT (Figure 5B–5C) and histology (Figure 5D–5E). No calcification was observed in the folded ePC-UPy polymer by any analytic technique at 21 days (Figure 5).

DISCUSSION

The present study showed distinctly different *in vivo* responses to four different biomaterials in a rat subcutaneous implantation model. The differences in tissue response to each material are summarized schematically in Figure 6. Of note, the host responses observed in this model were consistent with established outcomes in large animal and clinical studies. In particular, the UBM-ECM scaffold showed a predominately M2-like macrophage phenotype that was accompanied by degradation of the scaffold and deposition of *de novo* tissue with abundant neovascularization, which is indicative of a constructive remodeling outcome[22] and has consistently been shown in multiple large animal preclinical studies[23–26]. More specifically, in a sheep model of fascial repair, implanted UBM-ECM showed robust infiltration of macrophages throughout the material and evidence of scaffold remodeling at one month[25]. At six months post implantation, there was decreased inflammation, complete degradation of the material, and deposition of vascularized connective tissue akin to the temporal response to UBM-ECM in the rodent subcutaneous implant model used in the present study [25]. Implantation of PP mesh induced encapsulation of the fibers with macrophages and fibrous tissue indicative of the well-established foreign body reaction to non-degradable synthetic materials[26,27]. Consistent with previous reports in both preclinical and clinical applications, the PP mesh was associated with a pro-inflammatory macrophage response[28] that decreased in magnitude over time, but persisted throughout the study[27,29,30]. In a canine abdominal wall defect model Clarke et al. also reported some vascularization of the tissue adjacent to the fibrous capsule surrounding PP fibers, but the amount of vascularity was low relative to vascularization of an implanted ECM scaffold[26]. The bioabsorbable synthetic ePC-UPy material induced a more rapid and diffuse cellular infiltration, a macrophage phenotype profile more indicative of healthy healing tissue[31], persistent neovascularization, and less susceptibility to calcification than the bovine pericardial bioprosthetic GF-BP that is widely used in cardiovascular surgery. Similar to observations in the present study, a pulmonary valve conduit constructed with ePC-UPy leaflets showed neovascularization, gradually increasing infiltration of macrophages, and a low occurrence of leaflet calcification; whereas a bioprosthetic valved conduit had consistent calcification of the conduit and a paucity of macrophages on the surface of the implant at 6 months after implantation in sheep[15].

The role of macrophages in the host response to biomaterials

Biologic materials, particularly those derived from complete extracellular matrix (ECM), are largely associated with a pro-remodeling M2-like macrophage phenotype and favorable remodeling outcome[10,11]. However, chemical crosslinking of the ECM can have considerable detrimental effects upon the host-mediated remodeling response[10,32]. Synthetic materials, including PP surgical mesh, typically induce an M1-like macrophage response, chronic inflammation and the classic foreign body reaction[8]. It is now understood however, that this response can be modulated by micro-architecture, biomechanics, and surface

characteristics, among other biomaterial properties[33]. The molecular mechanisms that drive the macrophage response to a synthetic material are not fully understood. However, the findings of several studies that have investigated relationships between biomaterial characteristics and the nature of associated macrophage responses are summarized in Supplemental Table 1.

In the present study, the observed temporal and spatial pattern of pro-inflammatory TNFα$^+$ macrophages to the GF-BP was consistent with that of other studies in which chemically crosslinked biologic scaffolds have been investigated[10,32]. These findings differ markedly from the anti-inflammatory macrophage phenotype associated with both ePC-UPy and UBM-ECM in the present study, and other non-crosslinked ECM scaffolds studied previously[11,34].

Biomaterial-associated calcification

Calcification is the most important pathology limiting the long-term success of heart valve replacement with bioprosthetic valves[14,35]. Calcification of biomaterials in general is a complex and incompletely understood process that is thought to be regulated by three factors: (1) biological factors (local environment of function and recipient's metabolic state); (2) biomaterial factors (structure and chemistry of the substrate biomaterial); and (3) biomechanical factors (degree and locations of stress and strain)[35,36]. Pre-treatment with glutaraldehyde (as with GF-BP) is considered an important biomaterial factor for calcification of bioprosthetic tissue[37,38]. Calcification of synthetic non-porous polymers occurs predominantly at their surfaces and involves mechanisms different from those of tissue-based biomaterials[36,39,40].

The role of host cells in calcification of biomaterials is uncertain. However, multiple studies have associated increased macrophage infiltration to calcification of bioprosthetic valves[41] and native aortic valves[42,43], clinically significant processes with likely distinctly different mechanisms. Li *et al.* observed significantly more M1-like macrophages and higher expression of TNFα in calcified native aortic valves compared to noncalcified valves[42]. Pro-inflammatory cytokines produced by M1-like macrophages, such as TNFα, promote calcification of valvular interstitial cells *in vitro* through increased nuclear factor kappa B activation, bone morphogenetic protein 2 expression, and ALP activity[44,45]. Conversely, it is hypothesized that M2-like macrophages are protective against calcification by synthesizing increased inorganic pyrophosphate, a direct inhibitor of calcium phosphate deposition, and downregulating ALP expression[46]. In the present study, GF-BP was associated with a potentially more "calcification-promoting" pro-inflammatory macrophage phenotype, while the anti-inflammatory macrophages infiltrating the ePC-UPy polymer may have contributed to protection against calcific deposits[46].

Both intrinsic and extrinsic mineralization of a biomaterial are generally enhanced at the sites of intense mechanical stress[14,47], however the mechanism of stress-induced calcification is not fully understood. Mechanical stress induces expression of osteogenic genes in valve interstitial cells *in vitro* and this osteogenic effect is exacerbated in the presence of pro-inflammatory stimuli[48]. In the present study, and consistent with previous reports in both experimental and clinical contexts[49,50], calcification of the GF-BP material

was promoted by static stress. However, static stress did not promote calcification of the ePC-UPy polymer. Whether the absence of mechanically-induced calcification of the ePC-UPy material noted herein will translate to improved long term functionality of the synthetic polymer-based valve under the dynamic stress of blood flow is uncertain[17].

Role of the host response in endogenous tissue restoration

In situ tissue engineering, or ETR, is a concept in which selection of a biomaterial that elicits an appropriate host response is imperative for success[51]. In cardiovascular applications of ETR, an acellular restorative device must be fully functional upon implantation into the body, become infiltrated and populated by host cells, and remodel over time[52,53]. In the context of cardiovascular applications of ETR, a successful remodeling outcome must also be devoid of calcification. Valve materials that are unable to remodel, such as GF-BP, are susceptible to calcification and other modes of structural valve degeneration. Various materials have been investigated to support ETR of cardiovascular tissue, including decellularized matrices from donor valves[54,55], small intestinal submucosa[56,57], or *in vitro* engineered ECM[58,59], and synthetic bioabsorbable polymers[15,16,53,60]. The use of synthetic bioabsorbable materials like ePC-UPy to support heart valve ETR represents a distinctive and potentially tunable immunomodulatory approach to the treatment of valvular disease.

The progression of heart valve or other cardiovascular ETR involves an inflammatory response, followed by neotissue formation, remodeling and homeostasis [52]. Although there are still many uncertainties regarding the role of macrophage polarization in ETR, it has been postulated that monocyte differentiation towards pro-remodeling M2-like macrophages should be established early in the process to achieve stable tissue restoration[52]. Mechanical factors such as cyclic strain and shear stress are important determinants of macrophage differentiation. Tuning mechanical properties of scaffolds has been reported as an important tool to control remodeling outcomes, although degradation kinetics and scaffold microstructure may be equally important contributors, depending on the exact application[61].

Long term preclinical testing as a pulmonary interposition graft[16] and pulmonary valved conduit[15] demonstrated positive tissue remodeling and functional replacement of the implanted polymer with neotissue, with low propensity for calcification. This has prompted initial clinical studies using a RestoreX™ graft with similar composition to the ePC-UPy scaffold as an extracardiac conduit in children requiring a Fontan procedure[17] (clinicaltrials.gov number NCT02377674) and as a pulmonary valved conduit for RVOT reconstruction in children[62] (clinicaltrials.gov: NCT02700100 & NCT03022708). Finally, early preclinical application as an aortic valve has been reported as well[63].

Study limitations

The model of subcutaneous implantation in rats, as used in the present study, is well established[20,49,50,64] and generally predicts a calcification response similar to that observed in clinical specimens[49,65]. Weanling animals were used in this study because of their more active immune system[66], and rapid, robust calcification response[49]. The subcutaneous

implant model is more cost effective, less technically difficult and more reliable than valve replacement in large animals[67,68]. Nevertheless, the subcutaneous implantation model used in the present study does not subject the material to continuous blood flow, blood pressure or dynamic mechanical stress which could influence the cellular and calcification response[53,69].

CONCLUSION

The host inflammatory response elicited by GF-BP, ePC-UPy, UBM-ECM, and PP are distinctly different in a rat subcutaneous implant model. Notably, the elicited responses correlate well with the divergent remodeling outcomes observed in large animal and clinical studies[15,16,22,27], suggesting the potential predictive ability of this model. Relative to the tissue response to GF-BP, the ePC-UPy material platform may support a favorable remodeling response as evidenced by neovascularization, anti-inflammatory phenotype of infiltrating macrophages and absence of calcific deposits. The specific qualities of the ePC-UPy material that contributed to this host response are under investigation. Nevertheless, the results of this study provide optimism that the properties demonstrated in the subcutaneous implant model described herein will translate to clinical outcomes using the ePC-UPy material.

Supplementary Material

Refer to Web version on PubMed Central for supplementary material.

REFERENCES

1. Londono R & Badylak SF Factors which affect the host response to biomaterials. in Host Response to Biomaterials:The Impact of Host Response on Biomaterial Selection (ed. Badylak SF) 1–12 (Academic Press, 2015).
2. Joung YH Development of implantable medical devices: From an engineering perspective. Int. Neurourol. J. 17, 98–106 (2013). [PubMed: 24143287]
3. Parisi L, Toffoli A, Ghiacci G & Macaluso GM Tailoring the interface of biomaterials to design effective scaffolds. J. Funct. Biomater. 9, 1–31 (2018).
4. Williams D Biomaterials and biomedical materials. in Materials Today: Definitions of Biomaterials for the Twenty-First Century (eds. Williams D & Zhang X) 15–23 (Elsevier, 2019). doi:10.1016/B978-0-12-818291-8.00002-X.
5. Williams DF On the mechanisms of biocompatibility. Biomaterials 29, 2941–2953 (2008). [PubMed: 18440630]
6. Chung L, Maestas DR, Housseau F & Elisseeff JH Key players in the immune response to biomaterial scaffolds for regenerative medicine. Adv. Drug Deliv. Rev. 114, 184–192 (2017). [PubMed: 28712923]
7. Vasconcelos DP, Águas AP, Barbosa MA, Pelegrín P & Barbosa JN The inflammasome in host response to biomaterials: Bridging inflammation and tissue regeneration. Acta Biomater. 83, 1–12 (2019). [PubMed: 30273748]
8. Wolf MT et al. Macrophage polarization in response to ECM coated polypropylene mesh. Biomaterials 35, 6838–6849 (2014). [PubMed: 24856104]
9. Veiseh O et al. Size-and shape-dependent foreign body immune response to materials implanted in rodents and non-human primates. Nat Mater. 14, 643–651 (2015). [PubMed: 25985456]

10. Brown BN et al. Macrophage phenotype as a predictor of constructive remodeling following the implantation of biologically derived surgical mesh materials. Acta Biomater. 8, 978–987 (2012). [PubMed: 22166681]
11. Badylak SF, Valentin JE, Ravindra AK, McCabe GP & Stewart-Akers AM Macrophage phenotype as a determinant of biologic scaffold remodeling. Tissue Eng. Part A 14, 1835–42 (2008). [PubMed: 18950271]
12. Johnston DR et al. Long-term durability of bioprosthetic aortic valves: Implications from 12,569 implants. Ann. Thorac. Surg. 99, 1239–1247 (2015). [PubMed: 25662439]
13. Pineda Molina C et al. Comparison of the host macrophage response to synthetic and biologic surgical meshes used for ventral hernia repair. J. Immunol. Regen. Med. 3, 13–25 (2019).
14. Schoen FJ & Levy RJ Tissue heart valves: current challenges and future research perspectives. J. Biomed. Mater. Res. 47, 439–65 (1999). [PubMed: 10497280]
15. Bennink G et al. A novel restorative pulmonary valved conduit in a chronic sheep model: Mid-term hemodynamic function and histologic assessment. J. Thorac. Cardiovasc. Surg. 155, 2591–2601.e3 (2018). [PubMed: 29366582]
16. Brugmans M, Serrero A, Cox M, Svanidze O & Schoen FJ Morphology and mechanisms of a novel absorbable polymeric conduit in the pulmonary circulation of sheep. Cardiovasc. Pathol. 38, 31–38 (2020).
17. Bockeria LA et al. Total cavopulmonary connection with a new bioabsorbable vascular graft: First clinical experience. J. Thorac. Cardiovasc. Surg. 153, 1542–1550 (2017). [PubMed: 28314534]
18. Freytes DO, Stoner RM & Badylak SF Uniaxial and biaxial properties of terminally sterilized porcine urinary bladder matrix scaffolds. J. Biomed. Mater. Res. B. Appl. Biomater. 84B, 408–414 (2008).
19. Li H et al. Increased expression of FGF-21 negatively affects bone homeostasis in dystrophin/utrophin double knockout mice. J. Bone Miner. Res. 35, 738–752 (2020). [PubMed: 31800971]
20. Schoen FJ, Tsao JW & Levy RJ Calcification of bovine pericardium used in cardiac valve bioprostheses: Implications for the mechanisms of bioprosthetic tissue mineralization. Am J Pathol 123, 134–145 (1986). [PubMed: 2421577]
21. Saleeb SF et al. Accelerated degeneration of a bovine pericardial bioprosthetic aortic valve in children and young adults. Circulation 130, 51–60 (2014). [PubMed: 24756063]
22. Hodde J & Hiles M Constructive soft tissue remodelling with a biologic extracellular matrix graft: Overview and review of the clinical literature. Acta Chir. Belg. 107, 641–647 (2007). [PubMed: 18274177]
23. Amigo N et al. Urinary Bladder Matrix Scaffolds Promote Pericardium Repair in a Porcine Model. J. Surg. Res. 249, 216–224 (2020). [PubMed: 32001387]
24. Young DA, Jackson N, Ronaghan CA, Brathwaite CEM & Gilbert TW Retrorectus repair of incisional ventral hernia with urinary bladder matrix reinforcement in a long-term porcine model. Regen. Med. 13, 395–408 (2018). [PubMed: 29726304]
25. Young DA, McGilvray KC, Ehrhart N & Gilbert TW Comparison of in vivo remodeling of urinary bladder matrix and acellular dermal matrix in an ovine model. Regen. Med. 13, 759–773 (2018). [PubMed: 30182807]
26. Clarke KM et al. Intestine submucosa and polypropylene mesh for abdominal wall repair in dogs. J. Surg. Res. 60, 107–114 (1996). [PubMed: 8592400]
27. Klinge U, Klosterhalfen B, Müller M & Schumpelick V Foreign body reaction to meshes used for the repair of abdominal wall hernias. Eur. J. Surg. 165, 665–673 (1999). [PubMed: 10452261]
28. Nolfi AL et al. Host response to synthetic mesh in women with mesh complications. Am. J. Obstet. Gynecol. 215, 206.e1–206.e8 (2016). [PubMed: 27094962]
29. Bellón JM, Buján J, Contreras LA, Carrera-San Martín A & Jurado F Comparison of a new type of polytetrafluoroethylene patch (Mycro Mesh) and polypropylene prosthesis (Marlex) for repair of abdominal wall defects. J. Am. Coll. Surg. 183, 11–18 (1996). [PubMed: 8673302]
30. Thomas D, Demetres M, Anger JT & Chughtai B Histologic Inflammatory Response to Transvaginal Polypropylene Mesh: A Systematic Review. Urology 111, 11–22 (2018). [PubMed: 28823633]

31. Koh TJ & DiPietro LA Inflammation and wound healing: the role of the macrophage. Expert Rev. Mol. Med. 13, 1–12 (2011).
32. Deeken CR et al. Histologic and biomechanical evaluation of crosslinked and non-crosslinked biologic meshes in a porcine model of ventral incisional hernia repair. J Am Coll Surg 212, 880–888 (2011). [PubMed: 21435917]
33. Rayahin JE & Gemeinhart RA Activation of macrophages in response to biomaterials. in Macrophages. Results and Problems in Cell Differentiation (ed. Kloc M) vol. 62 317–351 (Springer, Cham, 2017). [PubMed: 28455715]
34. Sadtler K et al. Divergent immune responses to synthetic and biological scaffolds. Biomaterials 192, 405–415 (2019). [PubMed: 30500722]
35. Siddiqui RF, Abraham JR & Butany J Bioprosthetic heart valves: Modes of failure. Histopathology 55, 135–144 (2009). [PubMed: 19694820]
36. Schoen FJ, Levy RJ, Tam H & Vyavahare N 2.4.5-Pathological calcification of biomaterials. in Biomaterials Science: An Introduction to Materials in Medicine (eds. Wagner WR, Sakiyama-Elbert SE, Zhang G & Yaszemski M) 973–994 (Academic Press, 2020). doi:10.1016/B978-0-12-816137-1.00065-9.
37. Golomb G et al. The role of glutaraldehyde-induced cross-links in calcification of bovine pericardium used in cardiac valve bioprostheses. Am. J. Pathol. 127, 122–130 (1987). [PubMed: 3105321]
38. Grabenwöger M et al. Impact of glutaraldehyde on calcification of pericardial bioprosthetic heart valve material. Ann. Thorac. Surg. 62, 772–777 (1996). [PubMed: 8784007]
39. Joshi RR et al. Calcification of polyurethanes implanted subdermally in rats is enhanced by calciphylaxis. J. Biomed. Mater. Res. 31, 201–207 (1996). [PubMed: 8731208]
40. Bernacca GM, Mackay TG, Wilkinson R & Wheatley DJ Polyurethane heart valves: fatigue failure, calcification, and polyurethane structure. J. Biomed. Mater. Res. 34, 371–379 (1997). [PubMed: 9086407]
41. Dahm M et al. Relevance of immunologic reactions for tissue failure of bioprosthetic heart valves. Ann. Thorac. Surg. 60, (1995).
42. Li G et al. The shift of macrophages toward M1 phenotype promotes aortic valvular calcification. J. Thorac. Cardiovasc. Surg. 153, 1318–1327.e1 (2017). [PubMed: 28283241]
43. Šteiner I, Krbal L, Rozkoš T, Harrer J & Laco J Calcific aortic valve stenosis: Immunohistochemical analysis of inflammatory infiltrate. Pathol. Res. Pract. 208, 231–234 (2012). [PubMed: 22436689]
44. Kaden JJ et al. Tumor necrosis factor alpha promotes an osteoblast-like phenotype in human aortic valve myofibroblasts: a potential regulatory mechanism of valvular calcification. Int. J. Mol. Med. 16, 869–872 (2005). [PubMed: 16211257]
45. Yu Z et al. Tumor necrosis factor-α accelerates the calcification of human aortic valve interstitial cells obtained from patients with calcific aortic valve stenosis via the BMP2-Dlx5 pathway. J. Pharmacol. Exp. Ther. 337, 16–23 (2011). [PubMed: 21205918]
46. Hénaut L et al. New insights into the roles of monocytes/macrophages in cardiovascular calcification associated with chronic kidney disease. Toxins (Basel). 11, 1–33 (2019).
47. Thubrikar MJ, Deck JD, Aouad J & Nolan SP Role of mechanical stress in calcification of aortic bioprosthetic valves. J. Thorac. Cardiovasc. Surg. 86, 115–125 (1983). [PubMed: 6865456]
48. Bogdanova M et al. Inflammation and mechanical stress stimulate osteogenic differentiation of human aortic valve interstitial cells. Front. Physiol. 9, (2018).
49. Levy RJ et al. Biologic determinants of dystrophic calcification and osteocalcin deposition in glutaraldehyde-preserved porcine aortic valve leaflets implanted subcutaneously in rats. Am. J. Pathol. 113, 143–155 (1983). [PubMed: 6605687]
50. Tsao JW, Levy RJ & Schoen FJ Compressive mechanical deformation inhibits calcification of bovine pericardium used in cardiac valve bioprosthesis. in The 13th Annual Meeting of the Society for Biomaterials 180 (1987).
51. Smits AIPM & Bouten CVC Tissue engineering meets immunoengineering: Prospective on personalized in situ tissue engineering strategies. Curr. Opin. Biomed. Eng. 6, 17–26 (2018).

52. Bouten CVC, Smits AIPM & Baaijens FPT Can we grow valves inside the heart? Perspective on material-based in situ heart valve tissue engineering. Front. Cardiovasc. Med. 5, 1–10 (2018). [PubMed: 29404341]
53. Kluin J et al. In situ heart valve tissue engineering using a bioresorbable elastomeric implant – From material design to 12 months follow-up in sheep. Biomaterials 125, 101–117 (2017). [PubMed: 28253994]
54. Sarikouch S et al. Early insight into in vivo recellularization of cell-free allogenic heart valves. Ann. Thorac. Surg. 108, 581–589 (2019). [PubMed: 30928547]
55. Iop L et al. Decellularized allogeneic heart valves demonstrate self-regeneration potential after a long-term preclinical evaluation. PLoS One 9, (2014).
56. Zafar F et al. Physiological growth, remodeling potential, and preserved function of a novel bioprosthetic tricuspid valve: Tubular bioprosthesis made of small intestinal submucosa-derived extracellular matrix. J. Am. Coll. Cardiol. 66, 877–888 (2015). [PubMed: 26293756]
57. Ruiz CE et al. Transcatheter placement of a low-profile biodegradable pulmonary valve made of small intestinal submucosa: A long-term study in a swine model. J. Thorac. Cardiovasc. Surg. 130, 477.e1–477.e9 (2005). [PubMed: 16077416]
58. Ballotta V, Driessen-mol A, Bouten CVC & Baaijens FPT Biomaterials Strain-dependent modulation of macrophage polarization within scaffolds. Biomaterials 35, 4919–4928 (2014). [PubMed: 24661551]
59. Weber B et al. Injectable living marrow stromal cell-based autologous tissue engineered heart valves: First experiences with a one-step intervention in primates. Eur. Heart J. 32, 2830–2840 (2011). [PubMed: 21415068]
60. Capulli AK et al. JetValve: Rapid manufacturing of biohybrid scaffolds for biomimetic heart valve replacement. Biomaterials 133, 229–241 (2017). [PubMed: 28445803]
61. Wissing TB, Bonito V, Bouten CVC & Smits AIPM Biomaterial-driven in situ cardiovascular tissue engineering—a multi-disciplinary perspective. npj Regen. Med. 2, 1–19 (2017). [PubMed: 29302338]
62. Morales DL et al. A novel restorative pulmonary valve conduit: Early outcomes of two clinical trials. Front. Cardiovasc. Med. 7, 1–9 (2021).
63. Miyazaki Y et al. Acute performance of a novel restorative transcatheter aortic valve: Preclinical results. EuroIntervention 13, e1410–e1417 (2017). [PubMed: 29061548]
64. Meuris B et al. A novel tissue treatment to reduce mineralization of bovine pericardial heart valves. J. Thorac. Cardiovasc. Surg. 156, 197–206 (2018). [PubMed: 29572021]
65. Fishbein MC et al. Calcifications of cardiac valve bioprostheses. Biochemical, histologic, and ultrastructural observations in a subcutaneous implantation model system. J. Thorac. Cardiovasc. Surg. 83, 602–609 (1982). [PubMed: 7062771]
66. Hachim D et al. Effects of aging upon the host response to implants. J. Biomed. Mater. Res. - Part A 105, 1281–1292 (2017).
67. Simionescu DT Prevention of calcification in bioprosthetic heart valves: Challenges and perspectives. Expert Opin. Biol. Ther. 4, 1971–1985 (2004). [PubMed: 15571459]
68. McGregor CGA, Carpentier A, Lila N, Logan JS & Byrne GW Cardiac xenotransplantation technology provides materials for improved bioprosthetic heart valves. J. Thorac. Cardiovasc. Surg. 141, 269–275 (2011). [PubMed: 21168032]
69. Meuris B, Ozaki S, Herijgers P, Verbeken E & Flameng W Bioprosthetic tissue calcification: Influence of blood contact and arterial pressure. An experimental study in rats and sheep. J. Heart Valve Dis. 12, 392–399 (2003). [PubMed: 12803341]

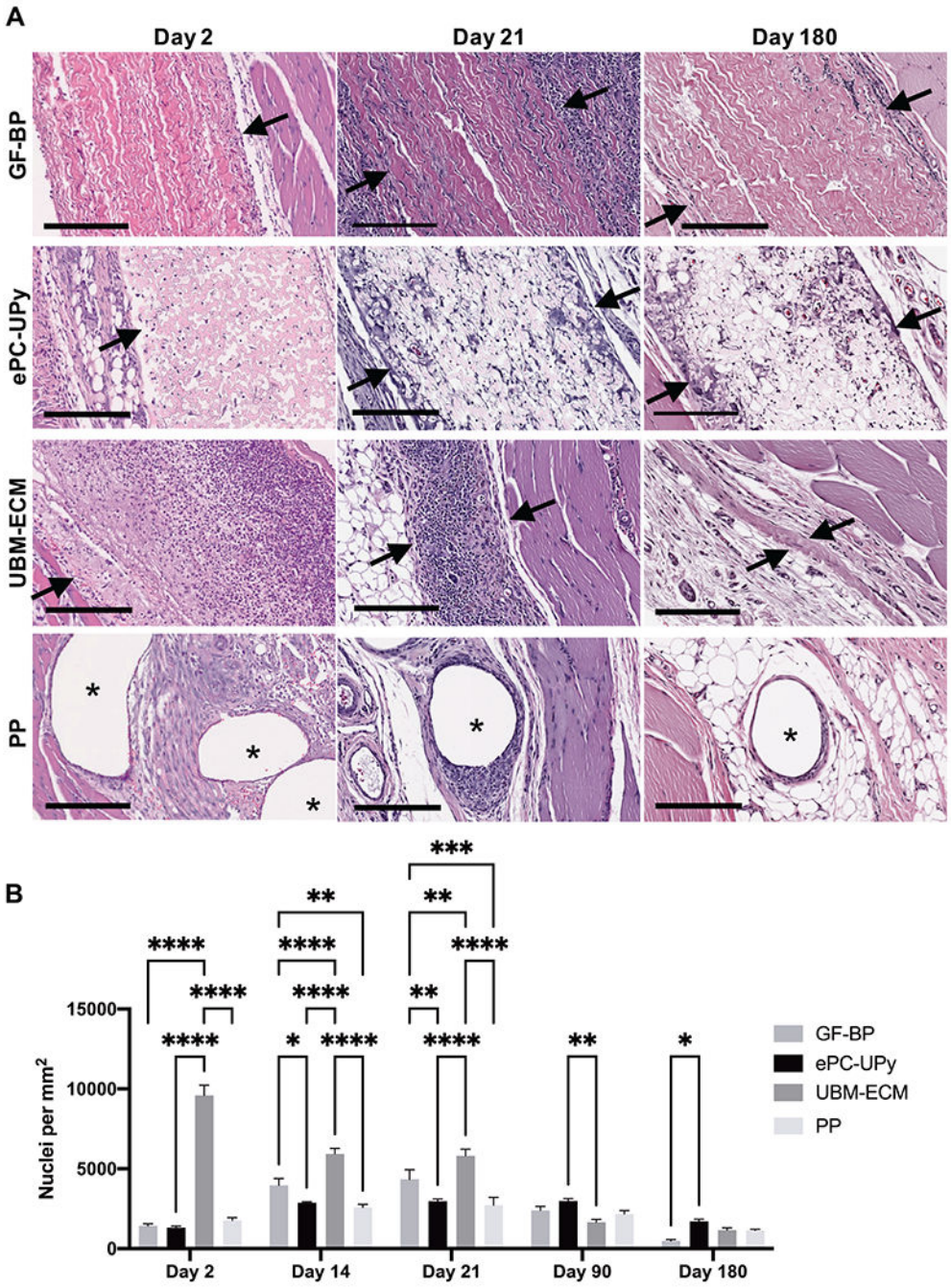

Figure 1. Cellular reactions to GF-BP, ePC-UPy, UBM-ECM, and PP.

(A) GF-BP, ePC-UPy, UBM-ECM, and PP at days 2, 21, and 180. (B) Quantification of total nuclei per mm^2 of material. With GF-BP, there was an early and robust cellular response, noted at 2 days post implantation with mononuclear cells limited to the edges of the implant at the interface with native tissue. There was a marked reduction in number of cells within GF-BP at 180 days. In contrast, beginning early following implantation and continuing throughout the study duration, mononuclear cells and occasional multinucleated giant cells were diffusely distributed throughout the thickness of the ePC-UPy material. UBM-

ECM showed a brisk mononuclear cell infiltration noted at 2 days post implantation and continuing through days 14-21 with disappearance of inflammation following degradation and replacement by fibrous tissue. Fibers of the PP mesh became rapidly surrounded by a variably thick cell layer of mononuclear and multinucleated giant cells that became thinner but persisted throughout the 180 days of the study. Arrows define the interface of the material with surrounding tissue, asterisks show PP fibers. All H&E stained, scale bars 200μm.

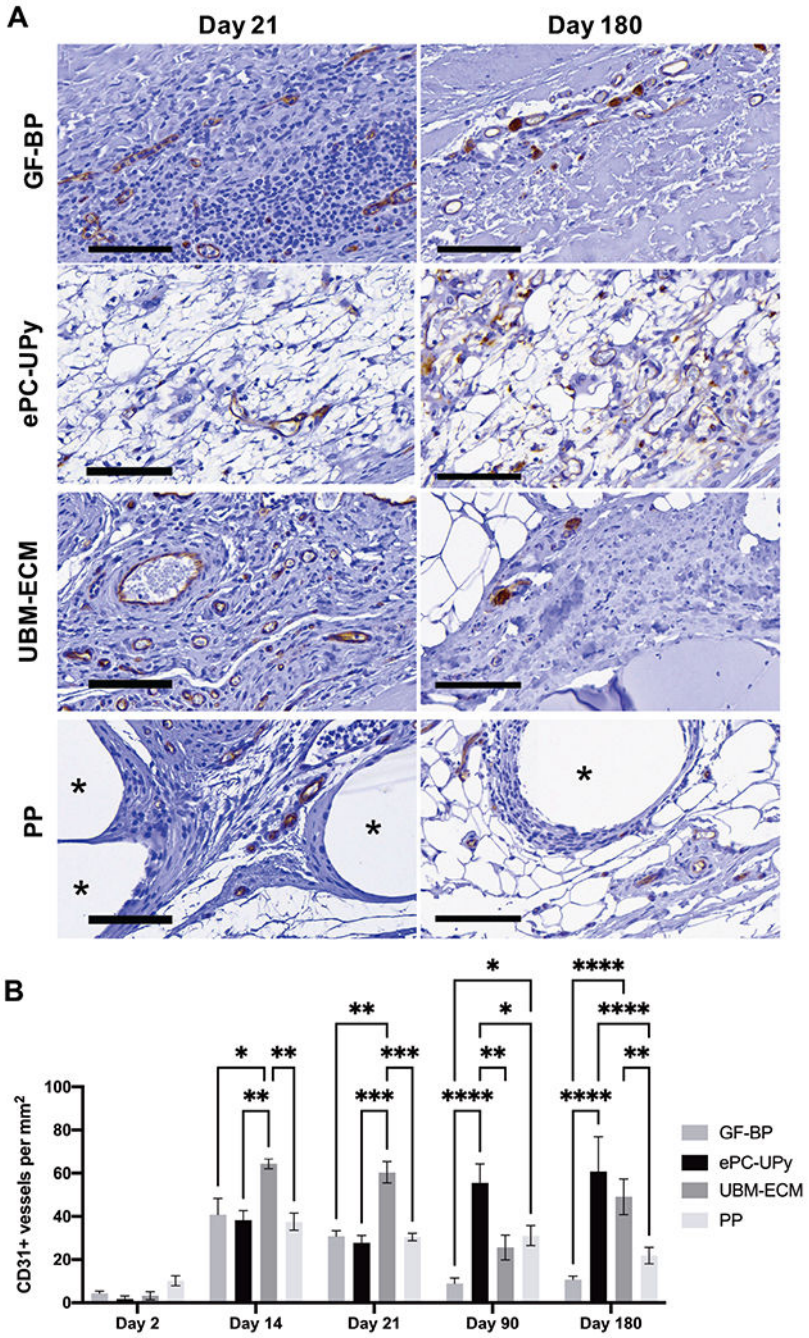

Figure 2. Endothelial cells and neovascularization in GF-BP, ePC-UPy, UBM-ECM, and PP.

(A) GF-BP, ePC-UPy, UBM-ECM, and PP at days 21, and 180 (B) Quantification of $CD31^+$ blood vessels per mm^2 of material. With GF-BP, $CD31^+$ endothelial cells were present scattered along the interface of GF-BP implant with surrounding tissue beginning early. However, microvessels with intraluminal RBC were found only on the edges of the material at 180 days post-implantation. At 14 days post-implantation, $CD31^+$ endothelial cells were identified within the ePC-UPy material consistent with neovascularization. By 90 and 180 days, a microvasculature that contained intraluminal RBC was noted within the ePC-UPy,

suggesting continuity of these blood vessels with the surrounding host tissue. Abundant neovascularization of the UBM-ECM scaffold was observed early after implantation as indicated by CD31 immunolabeling. Although $CD31^+$ cells were found in the surrounding cellular infiltrate of the PP mesh beginning at 14 days, neovascularization was not present outside of the dense cell layer encapsulating the fibers. All stained for CD31, scale bars 100μm.

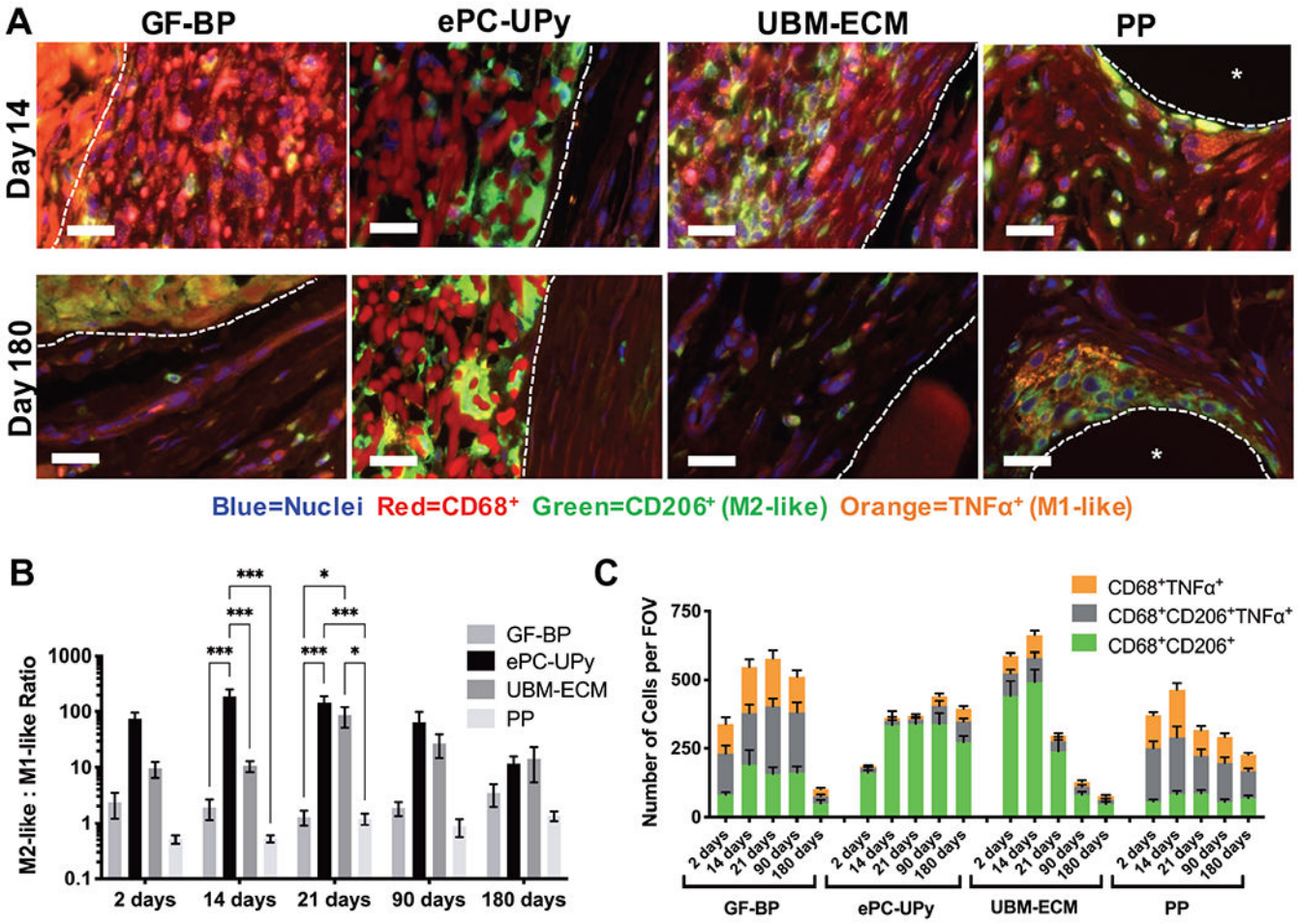

Figure 3. Macrophage response to GF-BP, ePC-UPy, UBM-ECM and PP.

(A) Representative images of immunolabeling of pan-macrophages ($CD68^+$, red), pro-remodeling M2-like macrophages ($CD206^+$, green) and pro-inflammatory M1-like macrophages ($TNF\alpha^+$, orange) at the 14 and 180 day timepoint. Scale bars 25um, dotted lines define the interface of the material, asterisk shows PP fiber. Biomaterial autofluorescence was not counted during quantification due to lack of co-localization with nuclei. (B) Quantification of the ratio of M2-like: M1-like ($CD68^+CD206^+$: $CD68^+TNF\alpha^+$) macrophages. Axis in log scale. (C) Quantification of the number of $CD68^+CD206^+$, $CD68^+CD206^+TNF\alpha^+$, and $CD68^+TNF\alpha^+$ macrophages per field of view. Macrophage immunolabeling indicates a dominant and sustained M2-like phenotype in response to the ePC-UPy material.

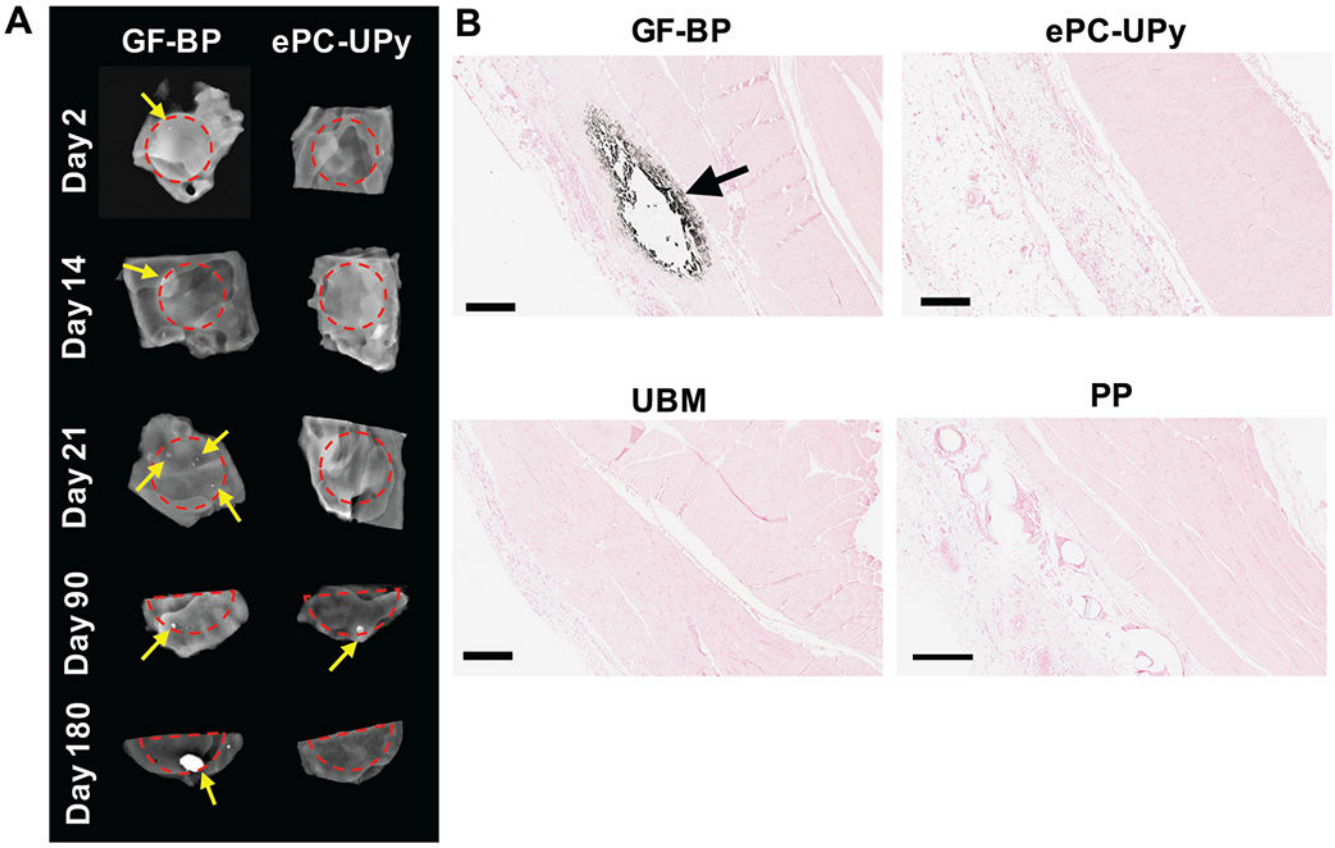

Figure 4. Susceptibility to calcification of GF-BP, ePC-UPy, UBM-ECM, and PP.

(A) Representative images of calcification within GF-BP and ePC-UPy as indicated by radiographic imaging. Red dotted lines define the edge of the material, yellow arrows indicate focal calcification. (B) Mineralization of GF-BP observed histologically by von Kossa (black arrow) and lack of mineralization observed in ePC-UPy, UBM-ECM, and PP at day 21. These comparisons indicate that the susceptibility to calcification often observed for bioprosthetic material, exemplified here for GF-BP, is absent with ePC-UPy, UBM-ECM and PP. (B) von Kossa stain, scale bars 400μm.

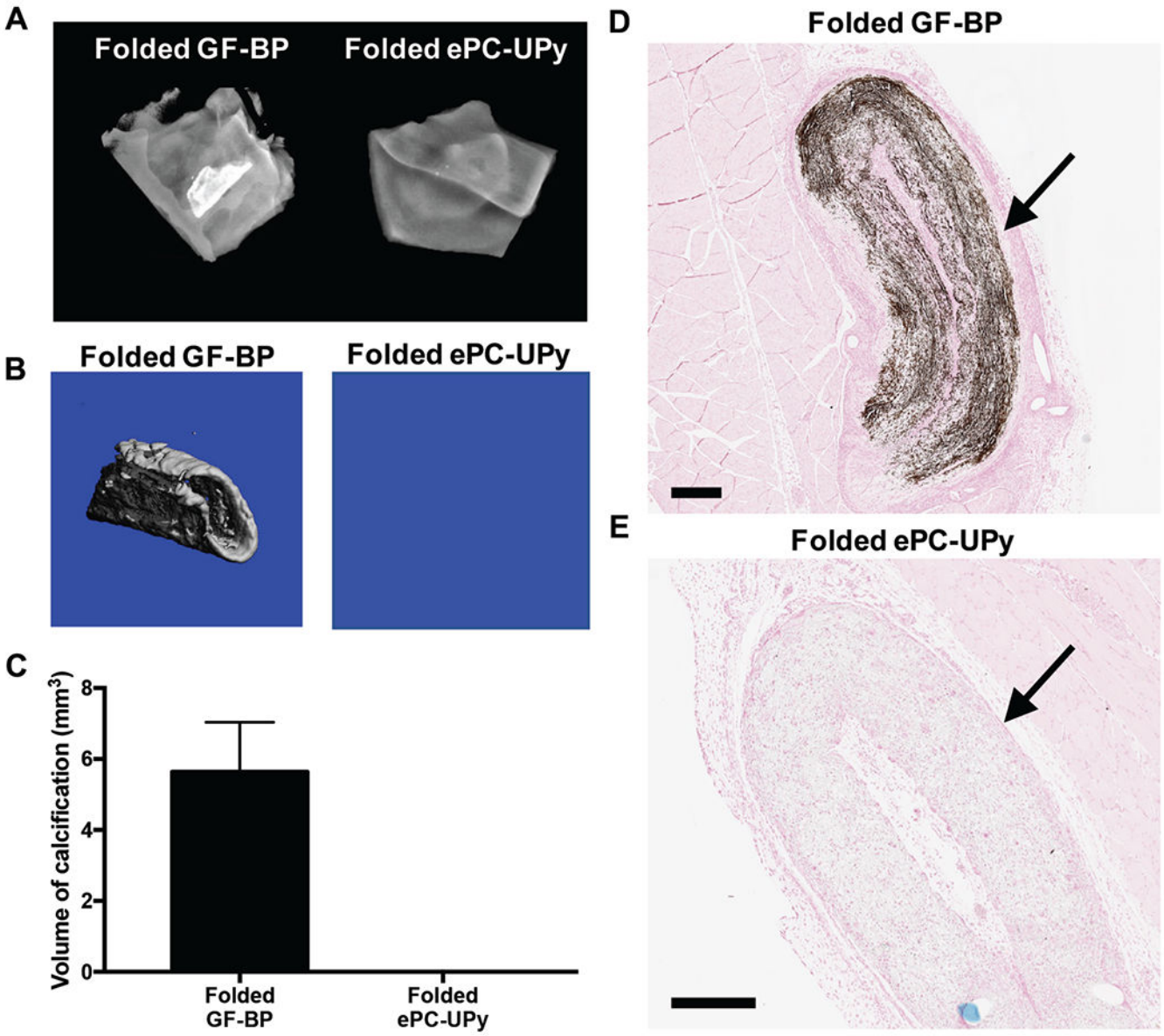

Figure 5. Susceptibility to mechanical stress induced calcification of GF-BP and ePC-UPy, as indicated by intentionally folded specimens.

(A) Representative radiographic images of calcification within folded test materials at 21 days. (B) Representative μCT scans of calcified areas within folded test materials. (C) Quantification of the volume of calcific nodules within each test material as determined by μCT analysis. (D) Mineralization within the folded GF-BP at 21 days as indicated by von Kossa. (E) Lack of mineralization within the folded ePC-UPy. Thus, the high susceptibility to mechanical stress-induced calcification in GF-BP was absent in ePC-UPy. (D) and (E) von Kossa stain, scale bars 400μm.

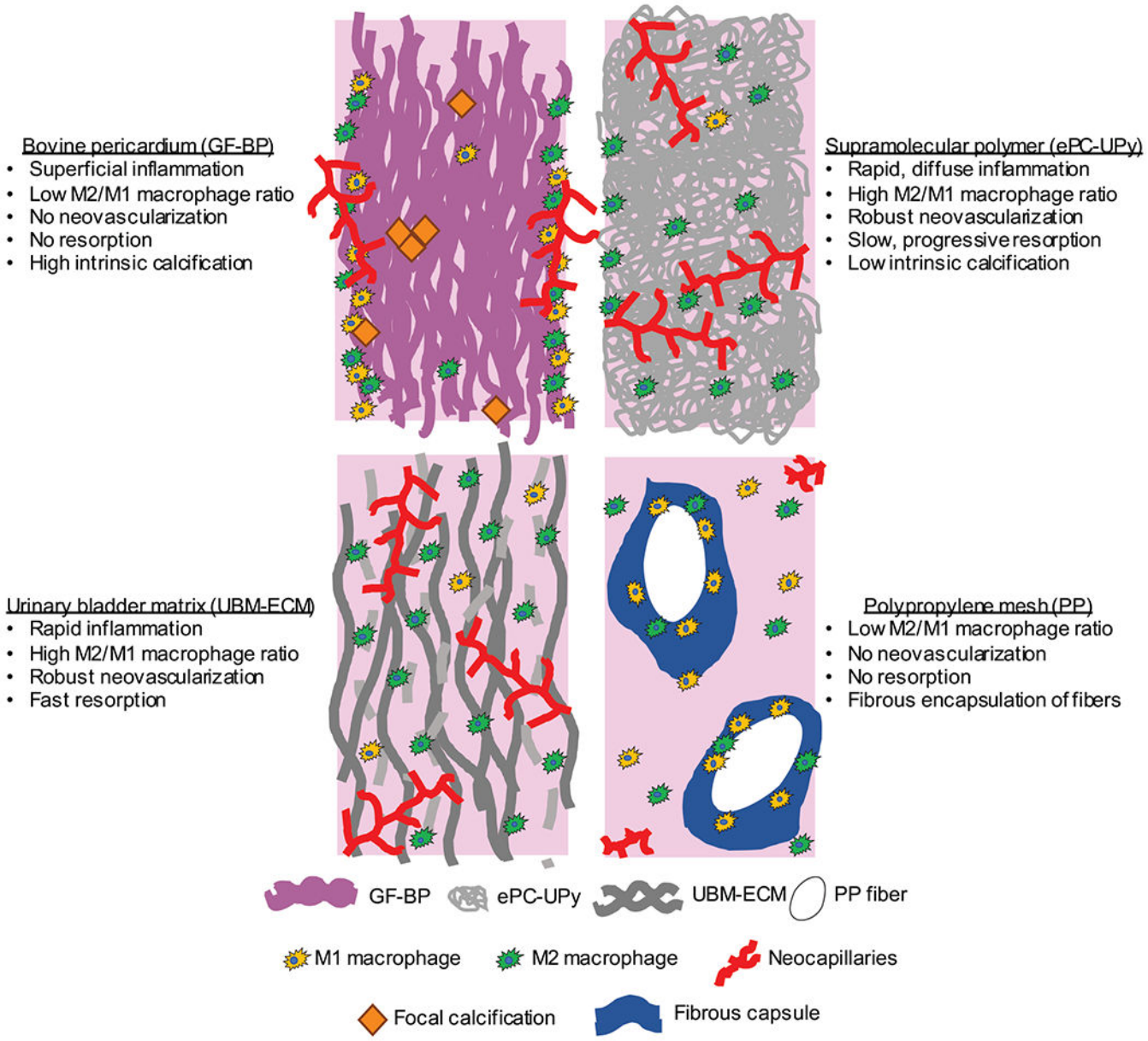

Figure 6.

Schematic summary of tissue responses to glutaraldehyde pre-treated bovine pericardium (GF-BP) bioprosthetic heart valve material, resorbable supramolecular polymer (ePC-UPy), urinary bladder extracellular matrix (UBM-ECM) and polypropylene mesh (PP) *in vivo*.